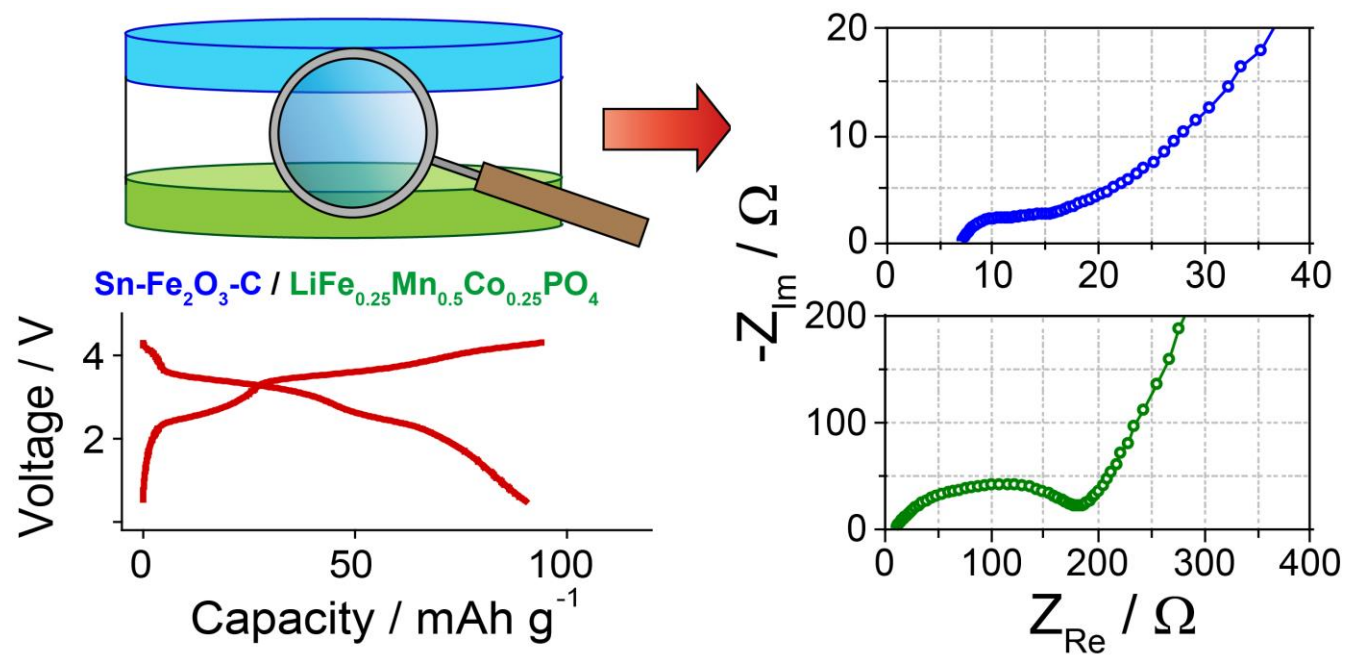


Graphical Abstract



Highlights

- New Li-ion batteries are reported
- $\text{LiFe}_{0.25}\text{Mn}_{0.5}\text{Co}_{0.25}\text{PO}_4$ olivine is used as the cathode
- Either Sn-C or Sn- Fe_2O_3 -C composites are used as anodes
- The electrode/electrolyte interfaces are monitored by EIS
- The systems are considered suitable for energy storage

1
2
3
4 **New lithium ion batteries exploiting conversion/alloying anode and $\text{LiFe}_{0.25}\text{Mn}_{0.5}\text{Co}_{0.25}\text{PO}_4$ olivine**
5
6
7 **cathode**

8
9
10 Daniele Di Lecce^a, Roberta Verrelli^a and Jusef Hassoun^{b*}

11
12
13 ^a Sapienza University of Rome, Chemistry Department, Piazzale Aldo Moro, 5, 00185, Rome, Italy

14
15 ^b Department of Chemical and Pharmaceutical Sciences, Chemistry, University of Ferrara,

16
17
18 Via Fossato di Mortara, 17, 44121, Ferrara, Italy

19
20 * Corresponding author: jusef.hassoun@unife.it

21
22
23
24 **Abstract**

25
26 New Li-ion cells are formed by combining a $\text{LiFe}_{0.25}\text{Mn}_{0.5}\text{Co}_{0.25}\text{PO}_4$ olivine cathode either with
27
28 Sn- Fe_2O_3 -C or with Sn-C composite anodes. These active materials exhibit electrochemical properties
29 particularly attractive in view of practical use, including the higher working voltage of the
30
31 $\text{LiFe}_{0.25}\text{Mn}_{0.5}\text{Co}_{0.25}\text{PO}_4$ cathode with respect to conventional LiFePO_4 , as well as the remarkable
32
33 capacity and rate capability of Sn- Fe_2O_3 -C and Sn-C anodes. The stable electrode/electrolyte interfaces,
34
35 demonstrated by electrochemical impedance spectroscopy, along with proper mass balancing and
36
37 anode pre-lithiation, allow stable galvanostatic cycling of the full cells. The two batteries, namely Sn-
38
39 Fe_2O_3 -C/ $\text{LiFe}_{0.25}\text{Mn}_{0.5}\text{Co}_{0.25}\text{PO}_4$ and Sn-C/ $\text{LiFe}_{0.25}\text{Mn}_{0.5}\text{Co}_{0.25}\text{PO}_4$, reversibly operate revealing
40
41 promising electrochemical features in terms of delivered capacity, working voltage and stability, thus
42
43 suggesting these electrodes combinations as suitable alternatives for an efficient energy storage.
44
45
46
47
48
49
50

51
52 **Keywords**

53
54 Olivine cathode; conversion; alloy anode; impedance spectroscopy; Li-ion battery

55
56
57
58 **Introduction**

1
2
3
4 Urgent need for improving conventional Li-ion battery science and technology, triggered by the
5
6 growing demand for energy storage, has promoted several studies on new electrodes exhibiting
7
8 enhanced features with respect to state of the art battery materials [1]. Accordingly, the main approach
9
10 for upgrading currently available electrodes is represented by the development of new chemistries and
11
12 compositions, leading to high values of the stored capacity [2] and working voltage [3]. Anodes
13
14 reacting by lithium alloying and conversion mechanisms have been proposed as viable candidates
15
16 characterized by remarkable specific capacity [4]. Among the various alloying materials (e.g. Si, Ge,
17
18 Sb, P, etc.) Sn represents a good compromise in terms of delivered capacity, material cost, toxicity,
19
20 volume strain upon cycling and safety [5–7]. Indeed, while the theoretical gravimetric capacity of Sn is
21
22 remarkably lower than the Si one (about 994 and 4200 mAh g⁻¹ for Sn and Si, respectively), their
23
24 theoretical volumetric capacities are not significantly different, being of 7233 mAh cm⁻³ and 8363
25
26 mAh cm⁻³ for Sn and Si, respectively. It is also worth mentioning that the very high specific
27
28 gravimetric capacity of Si anodes, largely exceeding that of the existing cathode materials, may be
29
30 disadvantageous in terms of cell balancing (i.e. anode loading, N/P ratio, etc.). In this respect, Sn
31
32 anodes may represent a more viable choice than Si in full lithium-ion battery configurations.
33
34 Furthermore, the volume change experienced by Sn upon reaction with Li⁺ is estimated to be of about
35
36 260 %, while Si is affected by a volume expansion of about 320%. Compared to Sb, Sn exhibits higher
37
38 theoretical specific capacity (about 4200 mAh g⁻¹ for Sn versus 660 mAh g⁻¹ for Sb) and comparable
39
40 volume change during charge/discharge, i.e. about 260% and 200% for Sn and Sb, respectively.
41
42 Moreover, Sn has a working voltage of about 0.3-0.4 V vs Li⁺/Li, which is lower than the one ascribed
43
44 to Sb (above 0.7 V vs Li⁺/Li [8]), thus suggesting Sn-based anodes as the preferred choice in full cells
45
46 configuration in terms of battery energy density. As for the cathode side, large attention has been
47
48 devoted towards materials with working voltages much higher than conventional LiCoO₂ and LiFePO₄
49
50 [9]. However, most of these studies have focused on the electrochemical characterization of the
51
52
53
54
55
56
57
58
59
60
61
62
63
64
65

1
2
3
4 materials in half-cell configuration employing lithium metal anode, while only limited number of
5
6 papers have demonstrated application in full Li-ion cells [5]. Indeed, the investigation of prototypes
7
8 using negative and positive Li-ion electrodes may actually proof the suitability of the materials, by
9
10 addressing concerns related to irreversible capacity, unstable solid electrolyte interface (SEI), and side
11
12 reactions leading to cell balance loss and consequent failure [5]. Therefore, further studies aimed at
13
14 determining the SEI layer stability and electrode reversibility are required in order to setup careful
15
16 negative to positive (N/P) mass ratio, thus allowing proper operation and suitable cycle life of the full
17
18 cell.
19
20
21

22
23 In this respect, we recently proposed new electrode materials for application in Li-ion battery based on
24
25 lithium alloying and conversion at the anode [10–13] and lithium insertion in $\text{LiFe}_{1-\alpha}\text{Me}_\alpha\text{PO}_4$ olivine at
26
27 the cathode [14,15]. In particular, Sn-C [10] and Sn- Fe_2O_3 -C [13] anodes have shown great reliability
28
29 and outstanding electrochemical performances while the $\text{LiFe}_{0.25}\text{Mn}_{0.5}\text{Co}_{0.25}\text{PO}_4$ composition has
30
31 revealed higher potential vs. Li^+/Li than common LiFePO_4 and, contemporary, relevant reversibility
32
33 and cycling ability. Following this trend, we study herein the characteristics of the materials in Sn-
34
35 C/ $\text{LiFe}_{0.25}\text{Mn}_{0.5}\text{Co}_{0.25}\text{PO}_4$ and Sn- Fe_2O_3 -C/ $\text{LiFe}_{0.25}\text{Mn}_{0.5}\text{Co}_{0.25}\text{PO}_4$ full cells. The ratio of this study
36
37 principally lies in the use of new electrode combinations characterized contemporary by good
38
39 electrochemical performances, as well as by expected low cost and environmental compatibility of the
40
41 employed materials. The Li-ion batteries are investigated by galvanostatic cycling and compared
42
43 focusing particular attention to the electrochemical characteristics of the electrode/electrolyte interface
44
45 inferred from electrochemical impedance spectroscopy (EIS) and to the electrodes tuning in terms of
46
47 N/P ratio.
48
49
50
51
52
53
54
55
56
57
58

59 **Experimental**

60
61
62
63
64
65

1
2
3
4 LiFe_{0.25}Mn_{0.5}Co_{0.25}PO₄, Sn-C, and Sn-Fe₂O₃-C samples were synthesized by following the procedures
5
6 previously reported [10,13,14]. The LiFe_{0.25}Mn_{0.5}Co_{0.25}PO₄ material consists of sub-micrometric
7
8 aggregates of elongated, platelet-like grains. Sn-C is composed by sphere-like Sn particles with an
9
10 average size ranging between 10 and 50 nm, dispersed in an amorphous Carbon matrix, with an overall
11
12 sub-micrometric sample morphology. The Sn-Fe₂O₃-C composite is formed by micrometric
13
14 agglomerates containing nanometric Sn (≤ 10 nm) and low crystallinity Fe₂O₃ particles dispersed
15
16 within carbon. The high purity degree of all the materials has been confirmed through XRD and EDS
17
18 measurements [10,13,14]. The electrode films were prepared by mixing active material, polymer binder
19
20 (PVdF-HFP Kynar Flex 2801 for the cathode and PVdF 6020 Solef Solvay for the anodes), and Super
21
22 P Carbon (Timcal) in the weight ratio 80:10:10 %. Tetrahydrofuran (Sigma-Aldrich) and N-methyl
23
24 pyrrolidone (Sigma-Aldrich) were used as solvents for cathode and anodes, respectively. The mixtures
25
26 were deposited on aluminum (cathode) and copper (anodes) foils by doctor blade, casted, and dried
27
28 under vacuum to obtain films of about 4 mg cm⁻² for LiFe_{0.25}Mn_{0.5}Co_{0.25}PO₄, 2.5 mg cm⁻² for Sn-C,
29
30 and 2 mg cm⁻² for Fe₂O₃-Sn-C. The electrodes were cut in the form of 10 mm diameter disks. T-type
31
32 cells were assembled in Ar-filled glovebox by stacking anode, Whatman separator soaked in 1 M LiPF₆
33
34 ethylene carbonate-dimethyl carbonate electrolyte (LP30, BASF), and cathode.
35
36
37
38
39
40
41
42

43 Electrochemical impedance spectroscopy (EIS) was carried out on three-electrode cell
44
45 configuration using a lithium probe as the reference electrode and a lithium disk as the counter
46
47 electrode. EIS was performed at open circuit voltage (OCV), after 1, 10, and 40 cycles of galvanostatic
48
49 cycling through a VersaSTAT MC Princeton Applied Research (PAR) analyzer, by applying a 10 mV
50
51 amplitude signal in the 500 kHz – 20 mHz frequency range. The EIS spectra were analyzed by
52
53 nonlinear least-square (NLLS) fit [16] by using the Boukamp program. Galvanostatic cycling were
54
55 performed on two-electrodes cells through a MACCOR series 4000 battery test system, with additional
56
57 constant voltage step for Sn-C/LiFe_{0.25}Mn_{0.5}Co_{0.25}PO₄. Prior to full-cells assembling, the anodes were
58
59
60
61
62
63
64
65

1
2
3
4 partially pre-lithiated by galvanostatic cycling in order to avoid first-cycle irreversible capacity and
5
6 ensure steady-state behavior. All the measurements were carried out at room temperature.
7
8
9

10 **Results and discussion**

11
12 The electrochemical features of the electrodes are studied by galvanostatic cycling and EIS
13
14 measurements. The electrochemical system used for the tests consists of a three electrode T-type cell
15
16 using a lithium foil reference probe, the active material as the working electrode and a lithium foil as
17
18 the counter electrode. This configuration contemporary allows suitable cycling behavior and proper
19
20 evaluation of the electrode/electrolyte interface by EIS (see the experimental section). Fig. 1 shows
21
22 respectively the voltage profiles and cycling trends of $\text{LiFe}_{0.25}\text{Mn}_{0.5}\text{Co}_{0.25}\text{PO}_4$ at C/5 rate ($1C = 170 \text{ mA}$
23
24 g^{-1} ; Fig. 1a, b), Sn-C at C/4 rate ($1C = 400 \text{ mA g}^{-1}$; Fig. 1c, d), and Sn- Fe_2O_3 -C at 1C rate ($1C = 810$
25
26 mA g^{-1} ; Fig. 1e, f), i.e., at current rates that ensure optimal cycling conditions. $\text{LiFe}_{0.25}\text{Mn}_{0.5}\text{Co}_{0.25}\text{PO}_4$
27
28 reveals in lithium cell an average working voltage of 3.9 V and delivers a capacity ranging from 80 to
29
30 90 mAh g^{-1} , i.e., a lower value with respect to that observed in two electrodes cell typically employed
31
32 for the galvanostatic tests (120 mAh g^{-1}) [7]. The lower value of delivered capacity may be reasonably
33
34 due to the differences between the three-electrodes and two-electrodes cell set-up (including, for
35
36 example, different amounts of electrolyte solution and employed separators). Furthermore, the lithium
37
38 probe used as reference electrode for the EIS tests in three-electrode configuration may alter the cell
39
40 geometry (increase of the thickness, change of the electric field), thus leading to a higher cell
41
42 polarization in galvanostatic cycling. This lithium probe is not employed for the cycling tests of Fig. 1
43
44 which is performed in a two-electrode configuration by using only the active material as the working
45
46 electrode and a lithium disk acting both as the reference and the counter electrode in a T-type cell (see
47
48 the experimental section for further details). Instead, Sn- Fe_2O_3 -C and Sn-C show a relevant
49
50 performance with average working voltage of about 0.5 V and 1 V, respectively, and reversible
51
52
53
54
55
56
57
58
59
60
61
62
63
64
65

1
2
3
4 capacity as high as 400 mAh g⁻¹ and 1000 mAh g⁻¹, i.e., values only slightly affected by the cell
5
6 configuration [10,11].
7
8
9

10 **Figure 1**

11
12 The EIS responses of the above discussed lithium cells, taken at the OCV and upon cycling, are
13 reported in Fig. 2. The Nyquist impedance plots have been analyzed by NNLS fit [16] using the
14
15 equivalent circuit reported in Table 1a, formed by high frequency resistive element describing the
16
17 ohmic electrolyte resistance, in series with high-middle sub-circuit element accounting for the
18
19 resistance and charge transfer pseudo-capacitance at the electrode-electrolyte interface layer, in series
20
21 with a low frequency Warburg element (Q_g) representative of the solid state Li⁺ diffusion within the
22
23 active material [17,18]. The sub-circuit element associated to the resistance and pseudo-capacitance of
24
25 the interface layer is composed by a series of three elements, each consisting in a resistive (R_i) and
26
27 pseudo-capacitance (Q_i) member connected in parallel. The attribution of each of these (R_iQ_i) elements
28
29 to a specific interface phenomenon may not be unambiguous. We suggest that the different anode
30
31 components, each exhibiting its characteristic particle size, crystallinity and chemical reactivity toward
32
33 the electrolyte, may account for different time constant interface phenomena, i.e. different high-middle
34
35 frequency semi-circles in the Nyquist plot. Indeed, the analysis of the interface phenomena we propose
36
37 for the tested composite anodes and the equivalent circuit accordingly used are in line with other
38
39 literature works on similar materials [19,20]. As for the cathode EIS characterization, a simpler
40
41 equivalent circuit is used to fit the obtained Nyquist plot. The interface phenomena are described by
42
43 one (RQ) element. Contributions of different components to the overall electrode-electrolyte interface
44
45 resistance and charge transfer pseudo-capacitance resulting in more semi-circles overlapped within the
46
47 same frequency region may not be excluded.
48
49
50
51
52
53
54
55
56
57
58
59
60
61
62
63
64
65

1
2
3
4 At the OCV condition all the electrodes show a single semicircle in the Nyquist plot, most
5 likely related to a native passivation layer (see Fig. 2a-c). The impedance response evolves by the
6 following cycles, owing to changes of the time-constants related to the interface phenomena, generally
7 leading to an additional medium-frequency semicircle due to electrode charge transfer. Further
8 medium-high semicircle may be ascribed to the heterogeneous nature of the composite electrode in
9 terms of particle size and coating thickness distribution [21–23], as indeed observed for Sn-C (Fig. 2b)
10 and Sn-Fe₂O₃-C (Fig. 2c). Possible overlapping of the semicircles at the medium and medium-high
11 frequency regions may be also observed, in particular for the LiFe_{0.25}Mn_{0.5}Co_{0.25}PO₄ cathode (Fig. 2a).
12 The results of NNLS fit, reported in Table 1, indicate for LiFe_{0.25}Mn_{0.5}Co_{0.25}PO₄ an increase of the
13 interfacial resistance from 180 Ω at the 1st cycle to 425 Ω at the 40th cycle, mostly due to the electrolyte
14 decomposition at the higher voltages (cell charge cutoff) and formation of favorable
15 electrode/electrolyte interface on the cathode surface, as indeed suggested by the corresponding cycling
16 trend (Fig 1b). Several factors may affect the evolution of the interface upon cycling, including the
17 decomposition of the electrolyte salt, possible nucleophilic attack of the electrolyte, oxygen release and
18 metal dissolution. Indeed, LiPF₆ may indeed decompose in presence of water leading to the formation
19 of LiF, PF₅ and HF, which may react at the cathode/electrolyte interface to form LiF-like species and
20 favor the transition metal dissolution [24]. The Nyquist plot of the Sn-C electrode (Fig. 2b) clearly
21 reveals lower resistance values, hence highlighting fast kinetics at the electrode/electrolyte interface.
22 The plots of Fig. 2b show a contribution of passivation layer and charge transfer to the overall interface
23 resistance, increasing from 18 Ω at the 1st cycle to 80 Ω at the 40th cycle (see Table 1b), i.e., values
24 ensuring a stable cycling (Fig. 1c, d).

25
26
27
28
29
30
31
32
33
34
35
36
37
38
39
40
41
42
43
44
45
46
47
48
49
50
51
52
53
54
55
56 The results of the NNLS fit of the impedance data, reported in Table 1, reveal that the overall interface
57 resistance of the ternary Sn-Fe₂O₃-C composite does not exhibit significant variation upon cycling: the
58 total resistance value is estimated to be as low as about 20-30 Ohm even after 40 galvanostatic cycles.
59
60
61
62
63
64
65

1
2
3
4 Although not being exhaustive, the EIS response upon prolonged cycling of the ternary Sn-Fe₂O₃-C
5
6 composite anode (reported in Fig. 2 c as Nyquist plot and in Table 1 as fitted resistance values) may
7
8 suggest reasonably high stability of the electrode SEI layer during cycling. Furthermore, considering
9
10 the very low overall resistance, i.e., of about 20 Ω for 40 cycles, evidenced by Fig. 2c we may expect a
11
12 well conducting Sn-Fe₂O₃-C/electrolyte interface, which accounts for the remarkable reversibility of
13
14 the electrode (about 1000 mAh g⁻¹, Fig. 1e, f).
15

16
17
18 Several works have investigated the SEI layer formed on the surface of Sn-based anodes. XPS and IR
19
20 measurements revealed that the SEI in conventional solutions of LiPF₆ salt in carbonate solvents
21
22 mainly consists of lithium alkyl-carbonates, RCO₂Li, ROLi, oligomers, Li₂CO₃ and LiF with
23
24 composition changing by cycles [24,25]. XPS and TOF-SIMS study on Sn-Co alloying electrodes has
25
26 revealed an increase of the Li₂CO₃ content in the SEI layer upon charge/discharge cycles as well as the
27
28 formation of fractures within the interface layers [26]. The exploitation of composite electrode
29
30 configurations, coatings or/and electrolyte additives may reasonably stabilize the SEI layer on the
31
32 electrode surface during cycling [27]. Indeed, the limited changes at increasing cycles of the Sn-C and
33
34 Sn-Fe₂O₃-C interface resistance values, as revealed from EIS measurements, proof the relatively high
35
36 stability of the interface layers formed by these electrodes upon prolonged cycling when electrolytes
37
38 based on LiPF₆ salt and carbonate solvents are used. This result is in line with other experimental
39
40 evidences reported in literature for similar composite materials [28,29].
41
42
43
44
45
46
47

48 **Figure 2**

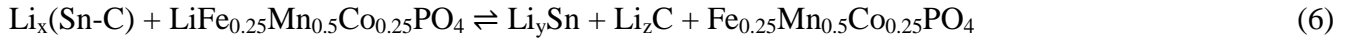
49
50 In summary, the interface characterization suggests the applicability of the electrode
51
52 combination in full cells with electrochemical features reflecting the anode and cathode properties.
53
54 Accordingly, the Sn-C and Sn-Fe₂O₃-C materials exchange lithium ions in electrochemical cells at
55
56 different potentials vs. Li⁺/Li with specific capacities of about 400 mAh g⁻¹ and 1000 mAh g⁻¹,
57
58 respectively, owing to the reaction mechanisms [10,13]:
59
60
61
62
63
64
65



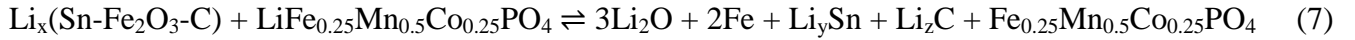
19
20 Mandatory steps to avoid full-cell irreversibility and ensure proper operation are represented by the
21 careful electrodes mass balancing and the optimization of a pre-lithiation procedure of the anode
22 [10,13]. Anode pre-lithiation before full cell assembly allows the formation of a stable SEI without
23 irreversible consumption of Li^+ at the cathode side, thus ensuring high reversibility and coulombic
24 efficiency of the battery even from the first cycles. The effects of pre-lithiation over the anode SEI
25 layer evolution upon cycling and the battery performances have been deeply investigated so far through
26 several techniques, including both in-situ and ex-situ analysis [30]. Both the Sn-C and Sn- Fe_2O_3 -C
27 anodes studied in this work are characterized by large irreversibility during the first cycles, which is in
28 part intrinsic to the alloying and conversion chemistry and, in part, is due to the electrolyte
29 decomposition reaction at the electrode surface with consequent formation of a SEI layer. Therefore,
30 the stabilization of these electrodes before full cell assembly by pre-lithiation process is of definite
31 importance in order to achieve satisfactory battery performances in terms of delivered capacity,
32 coulombic efficiency and cycle life. The pre-lithiation may be performed electrochemically by cycling
33 the electrodes in lithium half-cells until stationary working conditions are reached, i.e., the procedure
34 adopted in this work, or chemically by direct contact under pressing of the electrode with lithium metal
35 just before cell assembling [13,31].
36
37
38
39
40
41
42
43
44
45
46
47
48
49
50
51
52
53
54
55
56
57
58

59 Fig. 3a and b compare the voltage profile of $\text{LiFe}_{0.25}\text{Mn}_{0.5}\text{Co}_{0.25}\text{PO}_4$ with that of partially
60 lithiated Sn-C (a) and Sn- Fe_2O_3 -C (b). Prior to full-cell assembly, half cells were pre-cycled at current
61
62
63
64
65

1
2
3
4 rates allowing the maximum practical capacity of the electrodes, i.e., C/10, C/4, and 1C for
5
6 $\text{LiFe}_{0.25}\text{Mn}_{0.5}\text{Co}_{0.25}\text{PO}_4$, Sn-C, and Sn- Fe_2O_3 -C, respectively. The combination of anodes and cathode
7
8 profiles leads to the voltage signature of the two full-cells reported in Fig. 3c. The Sn- Fe_2O_3 -
9
10 C/ $\text{LiFe}_{0.25}\text{Mn}_{0.5}\text{Co}_{0.25}\text{PO}_4$ cell has a lower and more sloping voltage profile with respect to the Sn-
11
12 C/ $\text{LiFe}_{0.25}\text{Mn}_{0.5}\text{Co}_{0.25}\text{PO}_4$ one, as expected by the higher potential vs. Li^+/Li of the Fe_2O_3 conversion
13
14 reaction compared to Li-Sn alloying process [10,13]. Accordingly, different voltage cutoffs have been
15
16 set for cycling the above mentioned two full-cells. Despite the lower energy content of partially
17
18 lithiated $\text{Li}_x(\text{Sn-C})$ and $\text{Li}_x(\text{Sn-Fe}_2\text{O}_3\text{-C})$ in full cell (about 200 mAh g^{-1} and 450 mAh g^{-1} ,
19
20 respectively), the pre-cycling process allows the evolution of the anode reaction at the lower potentials
21
22 (Fig. 3a, b) and leads to higher voltage in full cells operating according to the reaction mechanisms:
23
24
25
26
27
28



$$(y = x + 1 - z \leq 4.4)$$



$$(y = x - 5 - z \leq 4.4)$$

29
30
31
32
33
34
35
36
37
38
39
40
41 The materials indicated by $\text{Li}_x(\text{Sn-C})$ and $\text{Li}_x(\text{Sn-Fe}_2\text{O}_3\text{-C})$ may contain lithiated alloying material and
42
43 carbon, lithium oxide or metallic iron, depending on the extent of the preliminary activation process of
44
45 the corresponding electrode.
46
47

Figure 3

48
49
50
51 Fig. 4 shows the galvanostatic behavior at C/5 rate with respect to the cathode mass ($1\text{C} = 170 \text{ mA g}^{-1}$)
52
53 of the Sn-C/ $\text{LiFe}_{0.25}\text{Mn}_{0.5}\text{Co}_{0.25}\text{PO}_4$ and Sn- Fe_2O_3 -C/ $\text{LiFe}_{0.25}\text{Mn}_{0.5}\text{Co}_{0.25}\text{PO}_4$ full-cells in terms of
54
55 voltage profiles (a, b) and cycling trends (c). Both panels a and b of Fig. 4 actually reveal the voltage
56
57 profile expected by the reactions (5) and (6), respectively, however with a progressive change by
58
59 cycling likely due to partial modification of the cell balance by minor irreversibility not completely
60
61
62
63
64
65

1
2
3
4 addressed by the pre-lithiation process. Fig. 4c indicates a relatively stable cycling trend for both the
5
6 Sn-C/LiFe_{0.25}Mn_{0.5}Co_{0.25}PO₄ and Sn-Fe₂O₃-C/LiFe_{0.25}Mn_{0.5}Co_{0.25}PO₄ configurations, with a steady
7
8 state reversible capacity ranging from 90 to 100 mAh g⁻¹ with respect to the cathode mass, thus
9
10 demonstrating the reliability of the two systems. Taking into account an average operating voltage of
11
12 about 3.5 and 3.2 V, and a correction factor for inactive materials contributions of 1/3, we may estimate
13
14 for Sn-C/LiFe_{0.25}Mn_{0.5}Co_{0.25}PO₄ and Sn-Fe₂O₃-C/LiFe_{0.25}Mn_{0.5}Co_{0.25}PO₄ cells a practical energy
15
16 density content of about 120 and 100 Wh kg⁻¹ for the, respectively, which is lower than the one
17
18 ascribed to commercial lithium-ion batteries based on graphite anode and LiCoO₂ and LiFePO₄
19
20 cathodes. However, the good electrochemical performances, the low cost and the environmental
21
22 compatibility of the electrodes well justify the study of the battery combination here proposed.
23
24
25
26
27

28 **Figure 4**

29 **Conclusions**

30
31
32 We proposed the combination of a new LiFe_{0.25}Mn_{0.5}Co_{0.25}PO₄ cathode material having olivine
33
34 structure with advanced conversion/alloying anodes as full Li-ion cells. The materials were studied by
35
36 using an electrochemical approach coupling impedance spectroscopy and galvanostatic cycling. The
37
38 results revealed suitable features of the electrode/electrolyte interface for LiFe_{0.25}Mn_{0.5}Co_{0.25}PO₄, Sn-C,
39
40 and Sn-Fe₂O₃-C. The Sn-C and Sn-Fe₂O₃-C anodes have different electrochemical characteristics, i.e.,
41
42 reversible capacities of about 400 and 1000 mAh g⁻¹, respectively, and voltage signatures reflecting the
43
44 Li/Sn alloying and Li/Fe₂O₃ conversion reactions. The Sn-C/LiFe_{0.25}Mn_{0.5}Co_{0.25}PO₄ and Sn-Fe₂O₃-
45
46 C/LiFe_{0.25}Mn_{0.5}Co_{0.25}PO₄ cells revealed voltage profiles resulting by proper cathode/anode mass
47
48 balance and anode partial pre-lithiation process. Despite the lower energy density with respect to the
49
50 benchmarks, the battery prototypes preliminarily studied in this work exhibit promising features that
51
52 may be optimized by further efforts aimed to improve the overall cycling performances and energy
53
54 density. Indeed, the LiFe_{0.25}Mn_{0.5}Co_{0.25}PO₄ cathode represents a more sustainable alternative to
55
56
57
58
59
60
61
62
63
64
65

1
2
3
4 conventional LiCoO₂ cathodes in terms of environmental impact and costs. It is also worth mentioning
5
6 that electrochemically de-lithiated LiCoO₂ is affected by poor thermal stability, with decomposition
7
8 starting at about 240°C (see ref. [32] for more details), which represents a major limit toward the
9
10 exploitation of its full capacity in practical batteries. When compared to conventional LiFePO₄, an
11
12 advantage of the LiFe_{0.25}Mn_{0.5}Co_{0.25}PO₄ cathode lies in its higher average working voltage, *i.e.* about
13
14 4.1 and 3.4 V vs Li⁺/Li for LiFe_{0.25}Mn_{0.5}Co_{0.25}PO₄ and LiFePO₄, respectively. As for the anode side,
15
16 the Sn-C and Sn-Fe₂O₃-C composites deliver very high values of reversible specific capacity (much
17
18 higher than that of conventional graphite electrodes of about 370 mAh g⁻¹). Moreover, these anodes are
19
20 prepared through simple and sustainable preparation routes and represent a viable and low cost choice
21
22 for application in batteries. Another advantage of these Sn-based anodes is represented by the high
23
24 safety level even at very high cycling rates, due to their working voltage preventing possible Li
25
26 deposition phenomena. Furthermore, the cell configuration proposed in this work may be attractive for
27
28 application requiring low temperatures (including, for example, the electric vehicles technology), *i.e.*,
29
30 under operative conditions that suppress the intercalation ability of conventional graphite anodes.
31
32 Therefore, the cells here proposed may be proposed by further optimization as alternative energy
33
34 storage systems of definite interest.
35
36
37
38
39
40
41
42
43

44 Acknowledgements

45
46
47 The work was performed within the collaboration project “Accordo di Collaborazione Quadro 2015”
48
49 between University of Ferrara (Department of Chemical and Pharmaceutical Sciences) and Sapienza
50
51 University of Rome (Chemistry Department).
52
53
54

55 References

- 56
57
58 [1] L. Croguennec, M.R. Palacin, Recent Achievements on Inorganic Electrode Materials for
59
60 Lithium-Ion Batteries, *J. Am. Chem. Soc.* 137 (2015) 3140–3156. doi:10.1021/ja507828x.
61
62
63

- 1
2
3
4 [2] B. Scrosati, J. Hassoun, Y.-K. Sun, Lithium-ion batteries. A look into the future, *Energy*
5
6 *Environ. Sci.* 4 (2011) 3287. doi:10.1039/c1ee01388b.
7
8
9
10 [3] M. Hu, X. Pang, Z. Zhou, Recent progress in high-voltage lithium ion batteries, *J. Power*
11
12 *Sources.* 237 (2013) 229–242. doi:10.1016/j.jpowsour.2013.03.024.
13
14
15 [4] J. Hassoun, B. Scrosati, Review—Advances in Anode and Electrolyte Materials for the Progress
16
17 of Lithium-Ion and beyond Lithium-Ion Batteries, *J. Electrochem. Soc.* 162 (2015) A2582–
18
19 A2588. doi:10.1149/2.0191514jes.
20
21
22
23 [5] V. Aravindan, Y.-S. Lee, S. Madhavi, Research Progress on Negative Electrodes for Practical
24
25 Li-Ion Batteries: Beyond Carbonaceous Anodes, *Adv. Energy Mater.* 5 (2015) 1402225.
26
27 doi:10.1002/aenm.201402225.
28
29
30
31 [6] S. Goriparti, E. Miele, F. De Angelis, E. Di Fabrizio, R. Proietti Zaccaria, C. Capiglia, Review
32
33 on recent progress of nanostructured anode materials for Li-ion batteries, *J. Power Sources.* 257
34
35 (2014) 421–443. doi:10.1016/j.jpowsour.2013.11.103.
36
37
38
39 [7] N. Nitta, G. Yushin, High-Capacity Anode Materials for Lithium-Ion Batteries: Choice of
40
41 Elements and Structures for Active Particles, Part. Part. Syst. Charact. 31 (2014) 317–336.
42
43 doi:10.1002/ppsc.201300231.
44
45
46
47 [8] T. Ramireddy, M.M. Rahman, T. Xing, Y. Chen, A.M. Glushenkov, Stable anode performance
48
49 of an Sb–carbon nanocomposite in lithium-ion batteries and the effect of ball milling mode in
50
51 the course of its preparation, *J. Mater. Chem. A.* 2 (2014) 4282. doi:10.1039/c3ta14643j.
52
53
54
55 [9] A. Kraytsberg, Y. Ein-Eli, Higher, Stronger, Better... □ A Review of 5 Volt Cathode Materials
56
57 for Advanced Lithium-Ion Batteries, *Adv. Energy Mater.* 2 (2012) 922–939.
58
59 doi:10.1002/aenm.201200068.
60
61
62
63
64
65

- 1
2
3
4 [10] J. Hassoun, G. Derrien, S. Panero, B. Scrosati, A Nanostructured Sn-C Composite Lithium
5
6 Battery Electrode with Unique Stability and High Electrochemical Performance, *Adv. Mater.* 20
7
8 (2008) 3169–3175. doi:10.1002/adma.200702928.
9
10
11 [11] R. Verrelli, J. Hassoun, A. Farkas, T. Jacob, B. Scrosati, A new, high performance
12
13 CuO/LiNi_{0.5}Mn_{1.5}O₄ lithium-ion battery, *J. Mater. Chem. A.* 1 (2013) 15329.
14
15
16 doi:10.1039/c3ta13960c.
17
18
19 [12] R. Verrelli, J. Hassoun, High-Capacity NiO-(Mesocarbon Microbeads) Conversion Anode for
20
21 Lithium-Ion Battery, *ChemElectroChem.* 2 (2015) 988–994. doi:10.1002/celec.201500069.
22
23
24 [13] R. Verrelli, J. Hassoun, High capacity tin–iron oxide-carbon nanostructured anode for advanced
25
26 lithium ion battery, *J. Power Sources.* 299 (2015) 611–616. doi:10.1016/j.jpowsour.2015.09.034.
27
28
29
30 [14] D. Di Lecce, R. Brescia, A. Scarpellini, M. Prato, J. Hassoun, A High Voltage Olivine Cathode
31
32 for Application in Lithium-Ion Batteries, *ChemSusChem.* 9 (2016) 223–230.
33
34
35 doi:10.1002/cssc.201501330.
36
37
38 [15] D. Di Lecce, J. Hassoun, Lithium Transport Properties in LiMn_{1- α} Fe _{α} PO₄ Olivine
39
40 Cathodes, *J. Phys. Chem. C.* 119 (2015) 20855–20863. doi:10.1021/acs.jpcc.5b06727.
41
42
43 [16] B.A. Boukamp, A Nonlinear Least Squares Fit procedure for analysis of immittance data of
44
45 electrochemical systems, *Solid State Ionics.* 20 (1986) 31–44. doi:10.1016/0167-2738(86)90031-
46
47
48
49
50
51
52
53 [17] D. Aurbach, Review of selected electrode–solution interactions which determine the
54
55 performance of Li and Li ion batteries, *J. Power Sources.* 89 (2000) 206–218.
56
57
58 doi:10.1016/S0378-7753(00)00431-6.
59
60 [18] B.-Y. Chang, S.-M. Park, Electrochemical Impedance Spectroscopy, *Annu. Rev. Anal. Chem.* 3
61
62
63
64
65

1
2
3
4 (2010) 207–229. doi:10.1146/annurev.anchem.012809.102211.
5
6

7 [19] C. Liu, H. Huang, G. Cao, F. Xue, R.A. Paredes Camacho, X. Dong, Enhanced Electrochemical
8 Stability of Sn-Carbon Nanotube Nanocapsules as Lithium-Ion Battery Anode, *Electrochim.*
9 *Acta.* 144 (2014) 376–382. doi:10.1016/j.electacta.2014.07.068.
10
11
12
13
14

15 [20] X. Huang, S. Cui, J. Chang, P.B. Hallac, C.R. Fell, Y. Luo, et al., A Hierarchical Tin/Carbon
16 Composite as an Anode for Lithium-Ion Batteries with a Long Cycle Life, *Angew. Chemie Int.*
17 *Ed.* 54 (2015) 1490–1493. doi:10.1002/anie.201409530.
18
19
20
21
22

23 [21] M.D. Levi, D. Aurbach, Impedance of a Single Intercalation Particle and of Non-Homogeneous,
24 Multilayered Porous Composite Electrodes for Li-ion Batteries, *J. Phys. Chem. B.* 108 (2004)
25 11693–11703. doi:10.1021/jp0486402.
26
27
28
29
30

31 [22] D. Aurbach, M.D. Levi, E. Levi, A review on the solid-state ionics of electrochemical
32 intercalation processes: How to interpret properly their electrochemical response, *Solid State*
33 *Ionics.* 179 (2008) 742–751. doi:10.1016/j.ssi.2007.12.070.
34
35
36
37
38

39 [23] S.-D. Xu, Q.-C. Zhuang, L.-L. Tian, Y.-P. Qin, L. Fang, S.-G. Sun, Impedance Spectra of
40 Nonhomogeneous, Multilayered Porous Composite Graphite Electrodes for Li-Ion Batteries:
41 Experimental and Theoretical Studies, *J. Phys. Chem. C.* 115 (2011) 9210–9219.
42
43
44
45
46
47
48
49
50
51
52
53
54
55
56
57
58
59
60
61
62
63
64
65

60 [24] M. Gauthier, T.J. Carney, A. Grimaud, L. Giordano, N. Pour, H.-H. Chang, et al., Electrode–
61 Electrolyte Interface in Li-Ion Batteries: Current Understanding and New Insights, *J. Phys.*
62 *Chem. Lett.* 6 (2015) 4653–4672. doi:10.1021/acs.jpcclett.5b01727.
63
64
65

60 [25] D.M. Seo, C.C. Nguyen, B.T. Young, D.R. Heskett, J.C. Woicik, B.L. Lucht, Characterizing
61 Solid Electrolyte Interphase on Sn Anode in Lithium Ion Battery, *J. Electrochem. Soc.* 162
62
63
64
65

- (2015) A7091–A7095. doi:10.1149/2.0121513jes.
- [26] J.-T. Li, J. Swiatowska, A. Seyeux, L. Huang, V. Maurice, S.-G. Sun, et al., XPS and ToF-SIMS study of Sn–Co alloy thin films as anode for lithium ion battery, *J. Power Sources*. 195 (2010) 8251–8257. doi:10.1016/j.jpowsour.2010.07.043.
- [27] N. Liu, Z. Lu, J. Zhao, M.T. McDowell, H.-W. Lee, W. Zhao, et al., A pomegranate-inspired nanoscale design for large-volume-change lithium battery anodes, *Nat. Nanotechnol.* 9 (2014) 187–192. doi:10.1038/nnano.2014.6.
- [28] Y. Xu, Q. Liu, Y. Zhu, Y. Liu, A. Langrock, M.R. Zachariah, et al., Uniform Nano-Sn/C Composite Anodes for Lithium Ion Batteries, *Nano Lett.* 13 (2013) 470–474. doi:10.1021/nl303823k.
- [29] G.A. Elia, U. Ulissi, F. Mueller, J. Reiter, N. Tsiouvaras, Y.-K.K. Sun, et al., A Long-Life Lithium Ion Battery with Enhanced Electrode/Electrolyte Interface by Using an Ionic Liquid Solution, *Chem. - A Eur. J.* 22 (2016) 6808–6814. doi:10.1002/chem.201505192.
- [30] M.W. Forney, M.J. Ganter, J.W. Staub, R.D. Ridgley, B.J. Landi, Prelithiation of Silicon–Carbon Nanotube Anodes for Lithium Ion Batteries by Stabilized Lithium Metal Powder (SLMP), *Nano Lett.* 13 (2013) 4158–4163. doi:10.1021/nl401776d.
- [31] J. Hassoun, K.-S. Lee, Y.-K. Sun, B. Scrosati, An advanced lithium ion battery based on high performance electrode materials., *J. Am. Chem. Soc.* 133 (2011) 3139–3143. doi:10.1021/ja110522x.
- [32] D. Di Lecce, C. Fasciani, B. Scrosati, J. Hassoun, A Gel–Polymer Sn–C/LiMn 0.5 Fe 0.5 PO 4 Battery Using a Fluorine-Free Salt, *ACS Appl. Mater. Interfaces.* 7 (2015) 21198–21207. doi:10.1021/acsami.5b05179.

1
2
3
4
5
6
7
8 **Table captions**
9

10 **Table 1.** (a) Equivalent circuit used for NNLS analysis of the EIS data (see Fig. 2) and (b) related
11 electrode/electrolyte interface resistances (R_i).
12
13

14
15
16 **Figure captions**
17

18 **Figure 1.** Galvanostatic cycling in three-electrodes lithium cells including lithium reference probe of
19 (a, b) $\text{LiFe}_{0.25}\text{Mn}_{0.5}\text{Co}_{0.25}\text{PO}_4$, (c, d) Sn-C, and (e, f) Sn- Fe_2O_3 -C in terms of (left panels) voltage
20 profiles of the 1st, 10th, and 40th cycles and (right panels) cycling behavior. For cell preparation see
21 experimental section
22
23
24
25
26
27

28 **Figure 2.** (a-c) Nyquist plots of EIS tests in three-electrodes lithium cells including lithium reference
29 probe of (a) $\text{LiFe}_{0.25}\text{Mn}_{0.5}\text{Co}_{0.25}\text{PO}_4$, (b) Sn-C, (c) Sn- Fe_2O_3 -C working electrodes; measurements
30 performed at OCV and after the 1st, 10th, and 40th cycles of galvanostatic cycling (see Fig. 1). For cell
31 preparation see experimental section
32
33
34
35
36
37

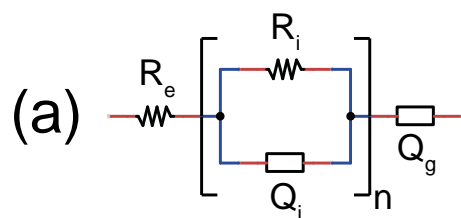
38 **Figure 3.** Voltage profile of $\text{LiFe}_{0.25}\text{Mn}_{0.5}\text{Co}_{0.25}\text{PO}_4$ cathode compared to partially lithiated Sn-C (a)
39 and to partially lithiated Sn- Fe_2O_3 -C (b). Surface geometric capacity of the cells reported in the bottom
40 x-axes, and the corresponding gravimetric capacity of the $\text{LiFe}_{0.25}\text{Mn}_{0.5}\text{Co}_{0.25}\text{PO}_4$ cathode in the top x-
41 axes. Current rates: C/10 for $\text{LiFe}_{0.25}\text{Mn}_{0.5}\text{Co}_{0.25}\text{PO}_4$ (1C = 170 mA g⁻¹), C/4 for Sn-C (1C = 400 mA
42 g⁻¹), and 1C for Sn- Fe_2O_3 -C (1C = 810 mA g⁻¹). (c) Voltage profile of the 20th, steady-state cycle for
43 the Sn-C/ $\text{LiFe}_{0.25}\text{Mn}_{0.5}\text{Co}_{0.25}\text{PO}_4$ and Sn- Fe_2O_3 -C/ $\text{LiFe}_{0.25}\text{Mn}_{0.5}\text{Co}_{0.25}\text{PO}_4$ cells, cycled at C/5 with
44 respect to the cathode mass (1C = 170 mA g⁻¹).
45
46
47
48
49
50
51
52
53
54
55
56

57 **Figure 4.** Galvanostatic performances of the Sn-C/ $\text{LiFe}_{0.25}\text{Mn}_{0.5}\text{Co}_{0.25}\text{PO}_4$ and Sn- Fe_2O_3 -
58 C/ $\text{LiFe}_{0.25}\text{Mn}_{0.5}\text{Co}_{0.25}\text{PO}_4$ cells at C/5 rate with respect to the cathode (1C = 170 mA g⁻¹). Voltage
59
60
61
62
63
64
65

1
2
3
4
5
6
7
8
9
10
11
12
13
14
15
16
17
18
19
20
21
22
23
24
25
26
27
28
29
30
31
32
33
34
35
36
37
38
39
40
41
42
43
44
45
46
47
48
49
50
51
52
53
54
55
56
57
58
59
60
61
62
63
64
65

profiles of the 2nd, 10th, 20th, 30th, and 40th cycles for (a) Sn-C/LiFe_{0.25}Mn_{0.5}Co_{0.25}PO₄ and (b) Sn-Fe₂O₃-C/LiFe_{0.25}Mn_{0.5}Co_{0.25}PO₄ cells and (c) comparison of the corresponding cycling trends.

Table 1



(b)

	LiFe_{0.25}Mn_{0.5}Co_{0.25}PO₄				Sn-C				Fe₂O₃-Sn-C			
	R ₁ (Ω)	R ₂ (Ω)	R ₃ (Ω)	R _{tot} (Ω)	R ₁ (Ω)	R ₂ (Ω)	R ₃ (Ω)	R _{tot} (Ω)	R ₁ (Ω)	R ₂ (Ω)	R ₃ (Ω)	R _{tot} (Ω)
OCV	30.1 ± 0.5			30.1 ± 0.5	25.6 ± 0.5			25.6 ± 0.5	52.2 ± 1.0			52.2 ± 1.0
1 st cycle	40 ± 30	140 ± 30		180 ± 60	1.9 ± 0.5	6.7 ± 0.9	9.0 ± 0.8	18 ± 2	3 ± 1	4 ± 4	16 ± 6	20 ± 10
10 th cycle	238 ± 3			238 ± 3	2.0 ± 0.9	21 ± 3	17 ± 3	40 ± 6	1.9 ± 0.7	4 ± 2	7 ± 2	12 ± 4
40 th cycle	425 ± 5			425 ± 5	2.8 ± 1	40 ± 5	42 ± 7	80 ± 10	2 ± 1	7 ± 5	8 ± 5	20 ± 10

Table 1

Figure 1

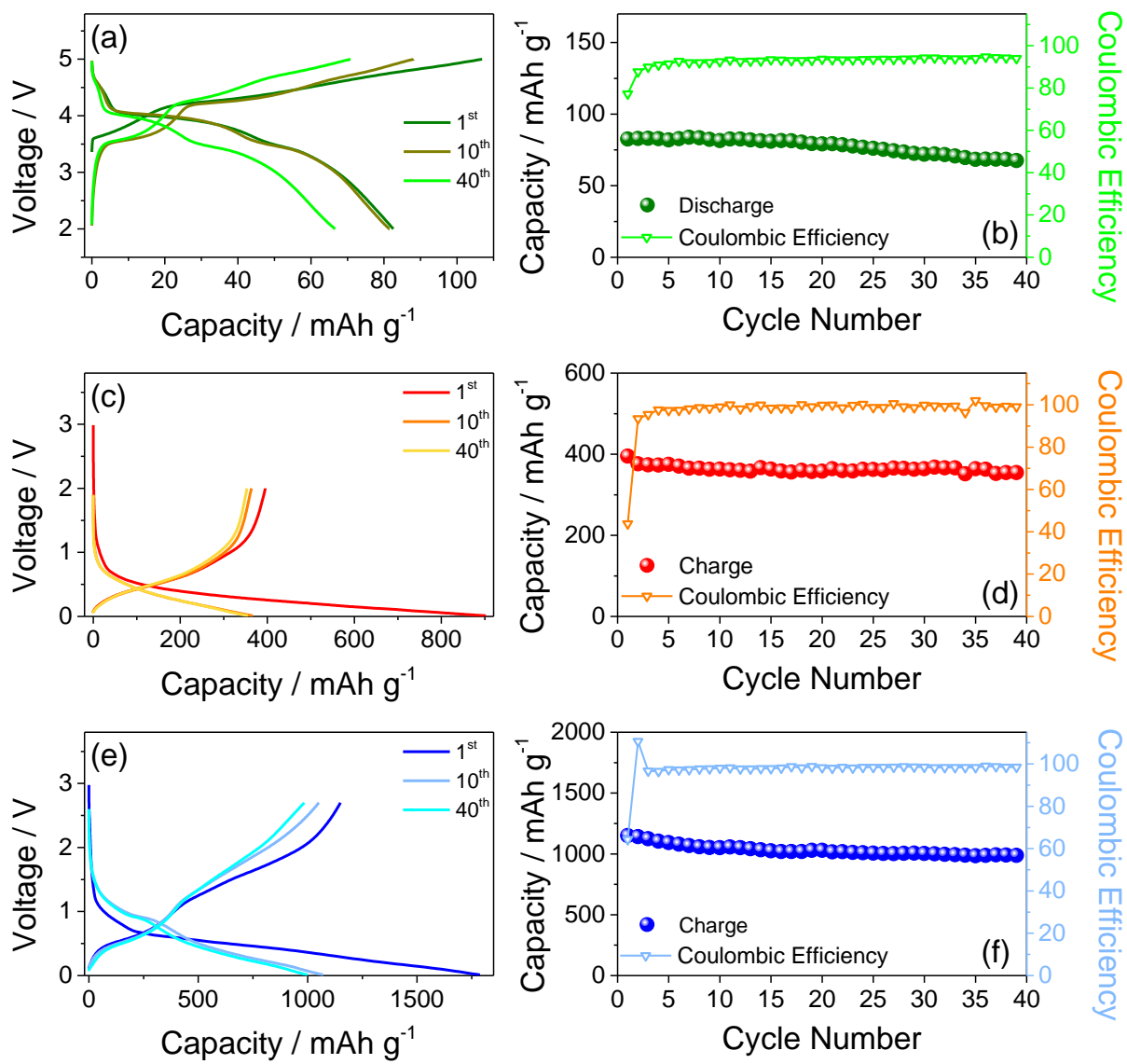


Figure 1

Figure 2

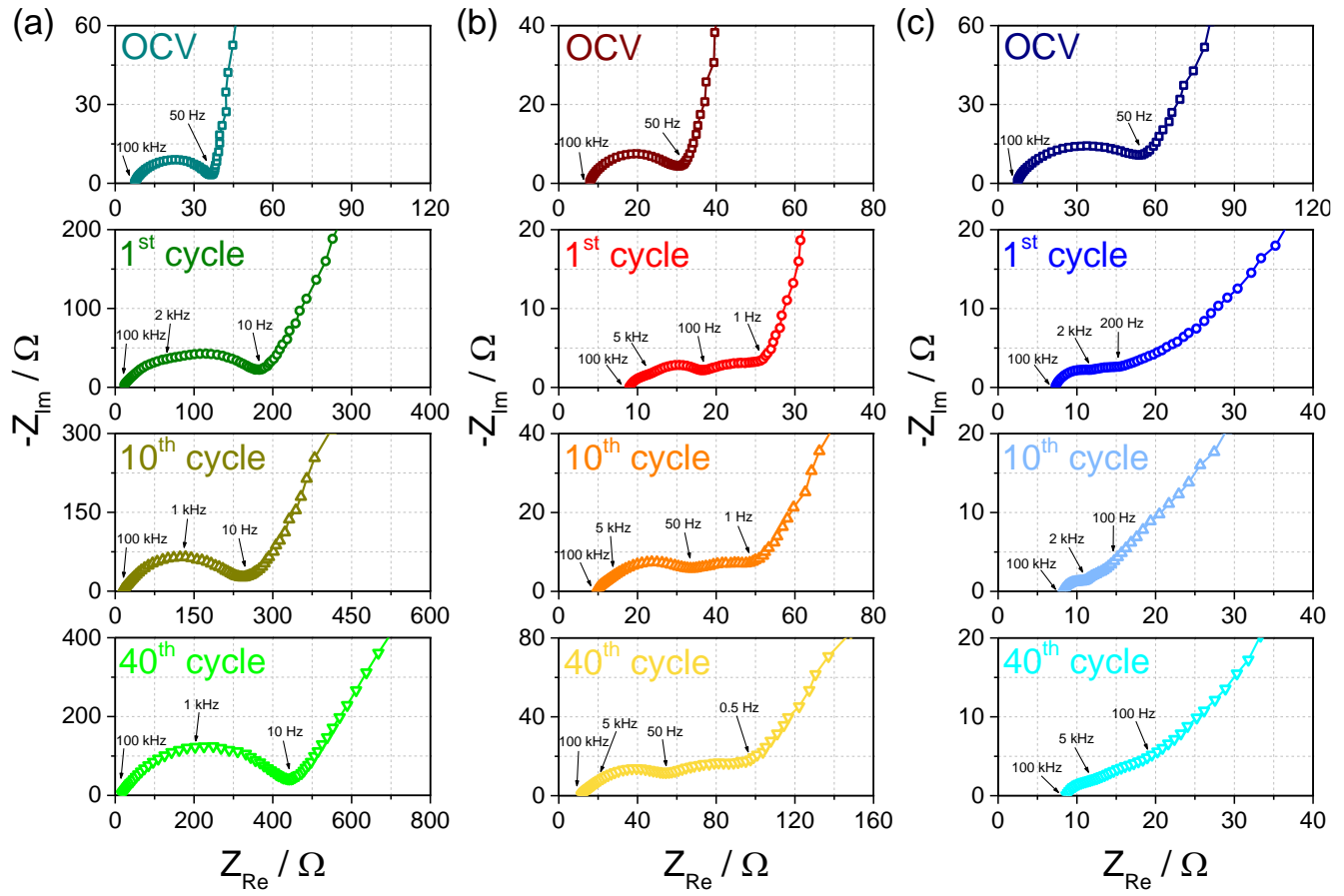


Figure 2

Figure 3

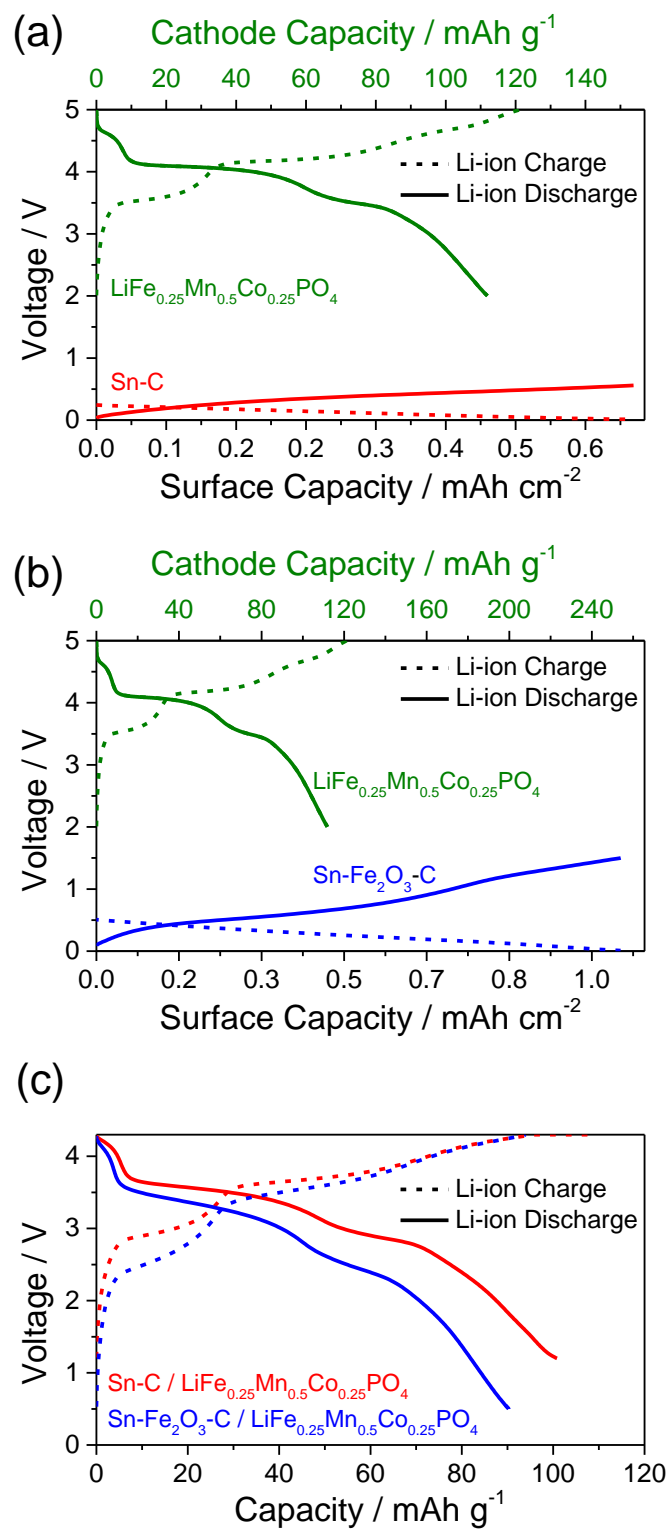


Figure 3

Figure 4

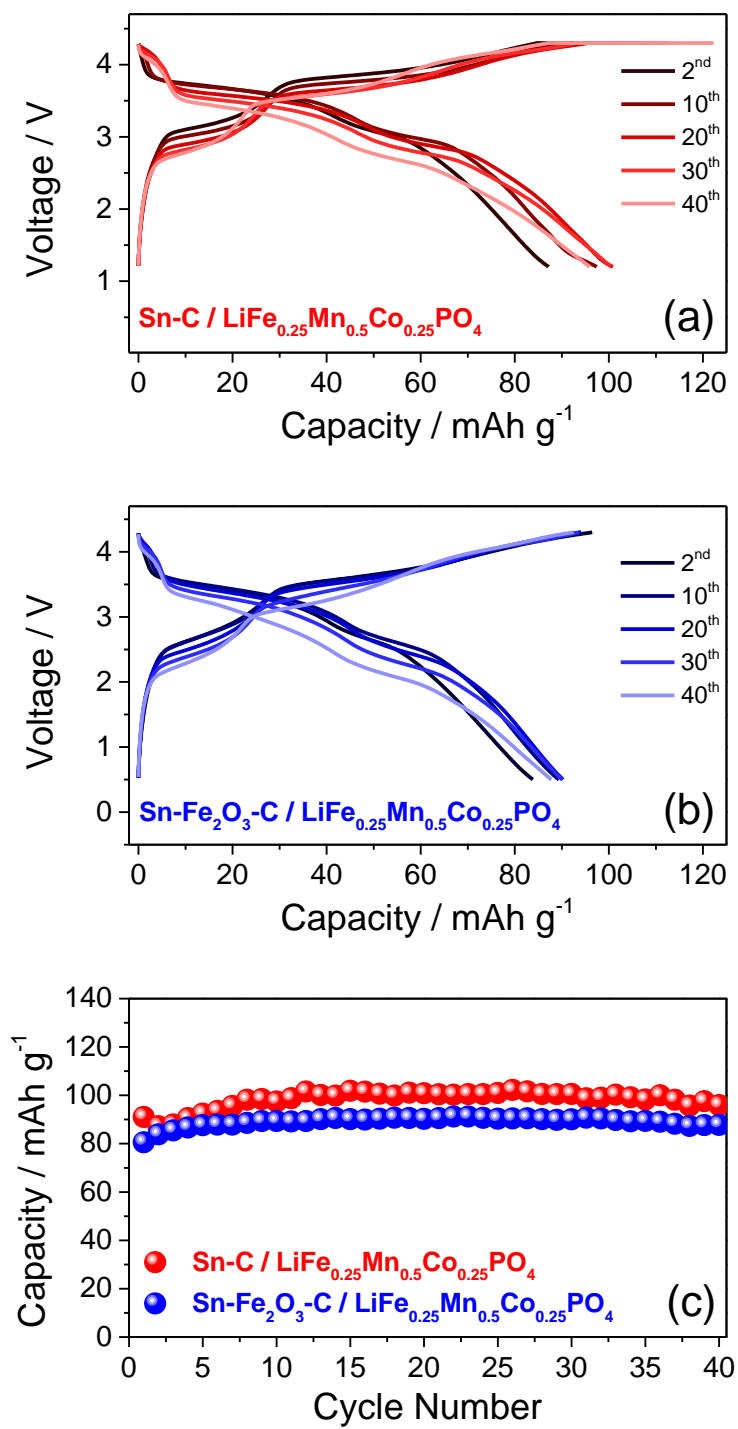


Figure 4